Mirrorless fused silica based double-prism monochromator for continuous measurements from near infrared to deep ultraviolet

THOMAS DITTRICH, [1,*] STEFFEN FENGLER, [2] AND MICHAEL FRANKE [3]

[1]*Helmholtz-Zentrum Berlin für Materialien und Energie GmbH, Schwarzschildstr. 8, D-12489 Berlin, Germany*
[2]*Freiberg Instruments GmbH, Delfter Str. 6, D-09599 Freiberg, Germany*
[3]*Elektronik Manufaktur Mahlsdorf, Paul-Wegener-Str. 36, D-12623 Berlin, Germany*
**dittrich@helmholtz-berlin.de*

Abstract: A mirrorless fused silica based double-prism monochromator was developed for continuous measurements over a wide spectral range. Lens positions were adjusted with respect to the spectral dependencies of the focal lengths. A guided optical rail has been implemented between both prisms. The monochromator enables measurements at photon energies between 0.4 and 7.3 eV. Straylight is suppressed by more than 8 orders of magnitude. Simulated and measured spectral resolutions are compared. Suitable applications of the monochromator were demonstrated for material characterization by photoelectron emission, optical transmission, photocurrent and surface photovoltage spectroscopy. The monochromator broadens the opportunities for the detection of defect states especially by surface photovoltage spectroscopy in ultra-wide bandgap semiconductors.

1. Introduction

Monochromators are standard optical instruments for the spectral dependent characterization of materials [1]. Photoelectric measurements of properties such as defect related transitions in semiconductors or work functions demand monochromatic light sources from the near infrared up to the deep ultraviolet at intermediate spectral resolution and very low straylight. A continuous light source with a spectral range between about 0.4 and 7.3 eV, i.e. between about 3100 and 170 nm, is desired with respect to values of semiconductor bandgaps and work functions. However, related continuous light sources are not available yet.

The heart of any monochromator is the dispersive element. Commercially available monochromators are based on diffraction gratings and mirror optics. A main advantage of a diffraction grating is that the dispersion can be precisely calculated [1]. For covering wide spectral ranges with a grating monochromator, diffraction gratings and order filters must be changed what causes discontinuities in measurements. For example, at least 4 diffraction gratings and order filters covering different spectral ranges are required for measurements with a grating monochromator between about 0.4 and 7.3 eV. Fused silica is transparent over a wide spectral range from about 0.4…0.5 to about 7…8 eV [2], depending on the specification of the fused silica. Furthermore, the dispersion of fused silica is usually well known [3]. Therefore, instead of 4 diffraction gratings and order filters, only one prism of fused silica is needed, allowing for continuous measurements over wide spectral ranges. In addition, strong suppression of straylight, which is demanded especially for the investigation of defect states in semiconductors, requires double or triple monochromators, i.e. a further doubling or tripling of dispersive elements. Incidentally, about sixty years ago, mirror monochromators with a fused silica prism, such as the SPM1 and SPM2 of Carl Zeiss Jena [4], were realized.

A main advantage of mirror optics is the absence of dispersion. However, coatings of mirror optics can introduce specific limitations and additional features in spectra. Therefore, mirror

optics are usually optimized for a specific spectral range, for example ultraviolet (UV). Lenses based on fused silica can be used over their whole transparency range without limitations or appearance of additional features. However, the focal length of lenses is a function of the spectral dependent dispersion of the material. Therefore, lenses based on fused silica are well suitable for the realization of mirrorless wide range monochromators whereas distances have to be individually adjusted with respect to the spectral dependencies of focal lengths.
This work is aimed to the development, characterization and demonstration of possible applications of a mirrorless fused silica based double-prism monochromator suitable especially for highly sensitive photoelectric measurements over a wide spectral range from about 0.4 to 7.3 eV at very low straylight. A ray tracer simulation program was created for optimizing the geometry and calculating the spectral resolution. Based on the simulations, Freiberg Instruments constructed and produced the prototype of a mirrorless fused silica based double-prism monochromator.

2. Ray-tracer simulations

Figure 1 (a) shows the optical scheme of the mirrorless fused silica based double-prism monochromator including the illumination unit with a lamp, a collimating lens (L1), a focusing lens (L2), the entrance slit, a collimating lens (L3), the first prism, a focusing lens (L4), the internal slit, a collimating lens (L5), the second prism, a focusing lens L6 and the exit slit. Both prisms rotate simultaneously. The optical axis of the lenses L4 and L5 is coupled with the rotation of the prisms by a guided optical rail centered at the position of the internal slit [5].

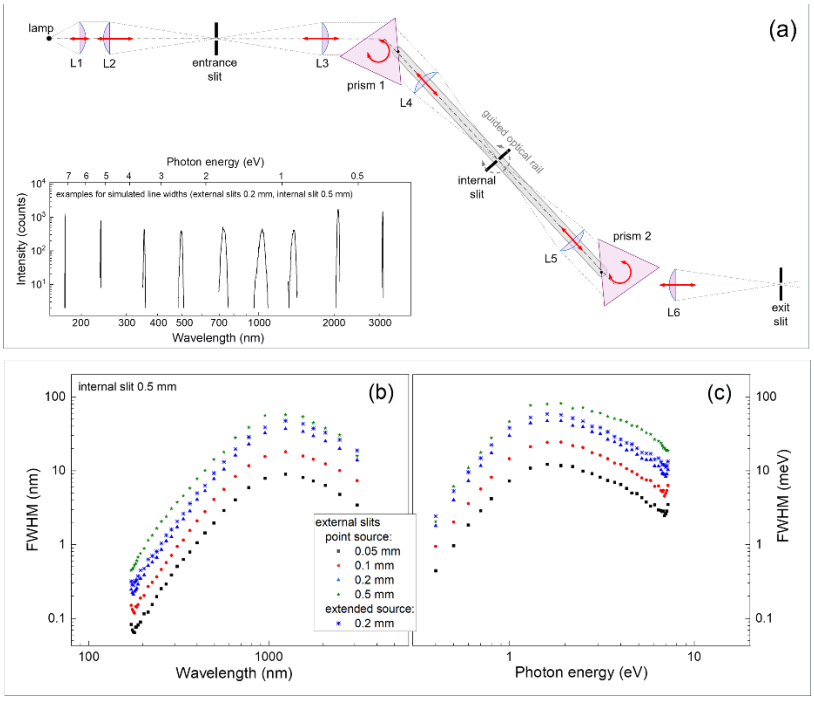

Fig. 1. Optical scheme of the mirrorless fused silica based double-prism monochromator with some simulated intensity spectra for external slits of 0.2 mm and an internal slit of 0.5 mm (insert) (a), spectral resolution as a function of wavelength (b) and photon energy (c) for a point source and external slits of 0.05, 0.1, 0.2 and 0.5 mm width (black squares, red circles, blue triangles and green stars, respectively) and for an extended source and external slits of 0.2 mm width (blue double crosses).

A ray-tracer simulation software was developed in order to find an optimal design for the mirrorless fused silica based double-prism monochromator. The design was aimed to get the monochromator as compact as possible, while still achieving a reasonable resolution by using lenses with nominal focus lengths of 150 mm (L2, L3, L6), 100 mm (L4, L5) and 50 mm (L1, aspheric), to cover a spectral range between 0.4 and 7.3 eV and to realize a spectral resolution of the order of several meV to several tens of meV depending on the spectral range. This intermediate range of spectral resolution was chosen as a compromise for getting a photon flux as high as possible at a resolution acceptable for analysis of transitions in photoelectric measurements of ultrawide bandgap semiconductors.

For the simulations of the monochromator, the variations of the spectral dependent focal lengths were considered between 110 and 165 mm, 73 and 110 mm, 36 and 55 mm for the nominal focus lengths of 150, 100 and 50 mm, respectively. In the simulation model, diffraction at the slits, reflections at walls and absorption lines in fused silica were not considered. A detector with a 2D spatial resolution was introduced at different positions along the optical path for optimizing the shape of the spot. Incidentally, optical distortions were compensated by the arrangement of the two prisms and the guided optical rail for lenses L4 and L5. For simulating the spectral range and resolution, a detector was placed behind the exit slit. The spectral resolution was found by varying the wavelength (photon energy) of simulated photons coming from the simulated light source, fixing the monochromator at a corresponding center wavelength and generating a histogram of the spectral dependent events at the detector. The spectral resolution was defined by the FWHM (full width at half maximum).

The insert of figure 1 (a) shows simulated intensity spectra for external slits of 0.2 mm width and an internal slit of 0.5 mm at 9 different peak wavelengths between 170 and 3100 nm, i.e. between 7.3 and 0.4 eV. The spectra demonstrate that the design of the monochromator is suitable for the variation of photon energies between 0.4 and 7.3 eV. The broadest spectrum, i.e. the lowest resolution, was obtained around 1100 nm (1.127 eV) whereas the spectra were much narrower at 170 and 3100 nm where the dispersion of fused silica is much higher. The spectra of the resolution are given as functions of wavelength and energy in figure 1 (b) and (c), respectively, for the central slit fixed at 0.5 mm width and varied width of external slits. For external slits of 0.05, 0.1 and 0.2 mm width, the FWHM scaled very well with the widths. For the external slit of 0.5 mm width, the influence of the internal slit became remarkable. For point and extended sources, the values of the FWHM at 1100 nm were 36 and 44 nm, respectively, for external slits of 0.2 mm width. In terms of photon energies at 0.4, 1.7 and 6 eV, i.e. at 3100, 729.4 and 206.7 nm, the values of the FWHM were 1.8, 48 and 13 meV, respectively, for external slits of 0.2 mm width.

The throughput or transmission is a further important characteristic of monochromators. The transmission of the mirrorless fused silica based double-prism monochromator has been simulated for widths of the external and internal slits of 0.2 and 0.5 mm, respectively, in the range between 0.4 eV (3100 nm) and 7.3 eV (169.7 nm). The transmission reached values between 1.6 % at 0.4 eV (3100 nm) and 21.8 % in the maximum at 6.5 eV (190.8 nm). An example screenshot with simulated pathways of photons and the complete simulated transmission spectrum of the mirrorless fused silica based double-prism monochromator are given in the appendix.

3. Prototype of the mirrorless fused silica based double-prism monochromator

A prototype (DPM100) of the mirrorless fused silica based double-prism monochromator has been constructed and manufactured by Freiberg Instruments precisely following the optimum geometry derived from simulations (figure 2 (a)). The illumination unit was adopted to a laser driven light source (LDLS, EQ-99X, Hamamatsu). The LDLS is a high-temperature light source and has a small, very stable and well-defined in space emission region with dimensions of the order of 100…200 µm. Therefore, the light of the LDLS can be well focused via the illumination unit onto the entrance slit of the monochromator. The lenses and the prisms were driven by stepper motors. For the tests, the widths of the slits were set to 0.2 mm (external slits) and 0.5 mm (internal slit).

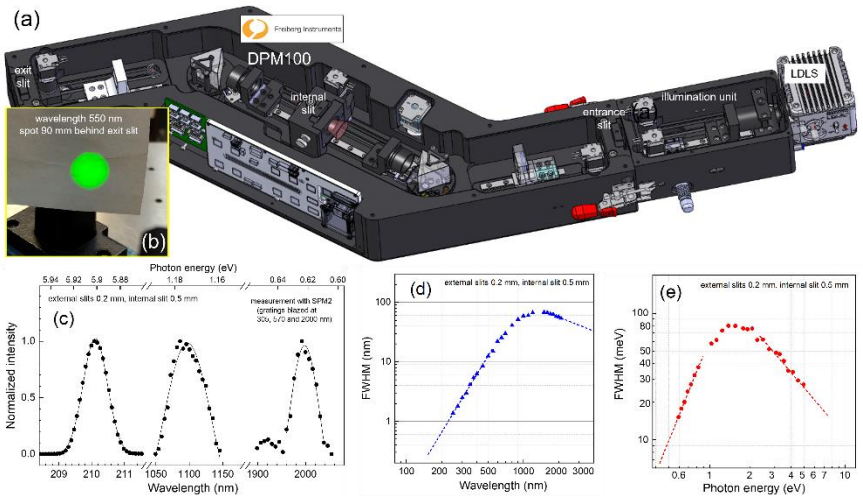

Fig. 2. Visualization of the CAD model of the open prototype of the mirrorless fused silica based double-prism monochromator (DPM100, Freiberg Instruments) with laser driven light source (LDLS) and illumination unit (a), photo of the light spot at 550 nm taken 90 mm behind the exit slit (b), resolution spectra at 210, 1100 and 2000 nm (external and internal slits 0.2 and 0.5 mm width, respectively) measured with a grating monochromator (c) and dependence of the FWHM in units of meV on photon energy (d). The dashed lines are approximations towards photon energies below and above the ranges covered by the grating monochromator.

As a typical example for the shape of the outcoming light spot, figure 2 (b) shows the photo of the light spot at 550 nm taken 90 mm behind the exit slit. The light spot fills homogenously a nearly ideal circle. This demonstrates the high quality of the design and configuration of the monochromator and the precise alignment of all optical elements.

The spectral resolution of the prototype of the mirrorless fused silica based double-prism monochromator was characterized by using a grating monochromator (SPM2 with gratings blazed at 305, 570 and 2000 nm) as a variable optical filter system. The gratings were calibrated with a calibration lamp (6035 Hg(Ar), Newport) by using characteristic lines in several orders. The entrance slit of the grating monochromator was placed directly behind the exit slit of the prototype of the mirrorless fused silica based double-prism monochromator. The slits of the grating were reduced so that the spectral resolution of the grating monochromator was much higher than that of the prototype of the mirrorless fused silica based double-prism monochromator. The signals were measured behind the exit slit of the grating monochromator with a silicon photodiode or a pyrodetector and the obtained calibration spectra were normalized against the intensity spectra of the DPM100.

Figure 2 (c) shows typical resolution spectra measured at 210, 1100 and 2000 nm. In the UV, the shapes of the resolution spectra could be well fitted by Gaussians. However, in the near infrared region, the shapes of the spectra were slightly asymmetric. The dependencies of the FWHM in units of nm and meV on wavelength and photon energy, respectively, are depicted

in figures 2 (d) and (e), respectively. The values of the FWHM in units of nm increased from about 1 nm at 200 nm to 65 – 70 nm between about 1150 and 1810 nm and decreased to about 40 nm at 3000 nm. The values of the FWHM in units of meV increased from about 7 meV at 0.5 eV to 80 meV between 1.38 and 1.65 eV and decreased to about 20 meV at 6 eV. The measured values of the FWHM are larger than the simulated values by about 30 – 40 %.

4. Intensity range and stray light of the mirrorless fused silica based double-prism monochromator

For highly sensitive measurements over wide spectral and intensity ranges, a highly sensitive 4-channel photodetector based on a UV-extended silicon photodiode (S15289-33, Hamamatsu) was developed for the measurement of signals over 210 dB without changing ranges during a measurement [6]. The photocurrent corresponds to the sum of 4 current-voltage converters with different sensitivity whereas the noise of the channels with lower sensitivity is discriminated. Figure 3 shows the photocurrent spectrum measured with the 4-channel photodetector over the full spectral range of the prototype of the mirrorless fused silica based double-prism monochromator. In the maximum (at 1.4 eV) and in the minimum (at 0.5 eV), the photocurrents were 52 µA and 80 fA, respectively. The noise and straylight levels cannot be precisely shown on a logarithmic scale. Therefore, the noise and straylight levels were measured independently (insert of figure 3). The average currents were 720 fA at 3000 nm and 620 fA in the dark. Therefore, since the spectral response of a silicon photodiode is zero at 3000 nm, the photocurrent caused by straylight was about 100 fA, what was about $5x10^8$ times smaller than the maximum photocurrent. This means that straylight is suppressed by more than 8 orders of magnitude by the prototype of the mirrorless fused silica based double-prism monochromator.

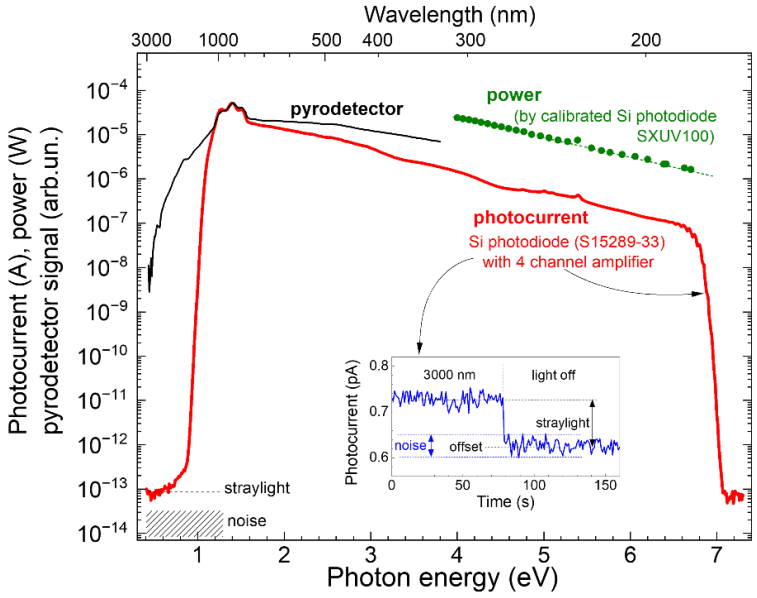

Fig. 3. Wide-range photocurrent spectrum measured with a 4-channel photodetector (red line, corrected to the offset), spectrum of a pyrodetector in arbitrary units (thin black line) and power in the UV-DUV (green circles). The insert shows the offset and the noise and stray light levels measured with the 4-channel photodetector under illumination at 3000 nm and in the dark. For this measurement, the monochromator was purged with nitrogen in order to reduce absorption by O_2 above 6.5 eV.

In the DUV, absorption by O_2 limited the spectral range (Schuman-Runge bands, [7]) of the mirrorless fused silica based double-prism monochromator. For the given measurements, the monochromator was purged with N_2 in order to reduce absorption by O_2 whereas Schuman-Runge bands could be still observed at higher photon energies. Strong absorption set on at photon energies above 6.7 eV (figure 3) and the photocurrent decreased to about 1 pA at 7 eV. The power of the outcoming light was measured with a photodiode (SXUV100, EQ photonics) calibrated in the UV-DUV range (PTB Berlin-Adlershof) between 4.0 and 6.7 eV (figure 3). The photocurrent of the SXUV100 was measured with a low noise current amplifier (DLPCA-200, Femto). The power decreased logarithmically with increasing photon energy from 24 µW at 4 eV to 1.7 µW at 6.7 eV.
The intensity spectrum measured with a pyrodetector (EMM) is shown in figure 3 (in arbitrary units), whereas the maximum has been aligned to the maximum photocurrent of the 4-channel photodetector. The intensity decreased towards lower photon energies was reduced by 1, 2 and 3 orders of magnitude at 1, 0.67 and 0.5 eV, respectively. The strong absorption by oxygen and hydroxide related defects in UV-grade fused silica and the steep incident angle for light at the prisms avoid remarkable light intensities below 0.5 eV [2].

5. Examples for application

Figure 4 illustrates some examples for possible applications of the mirrorless fused silica based double-prism monochromator. Possible applications are related to methods like PES, optical transmission spectroscopy, photocurrent spectroscopy and surface photovoltage spectroscopy (figures 4 (a) – (d), respectively) whereas each application highlights a certain aspect.

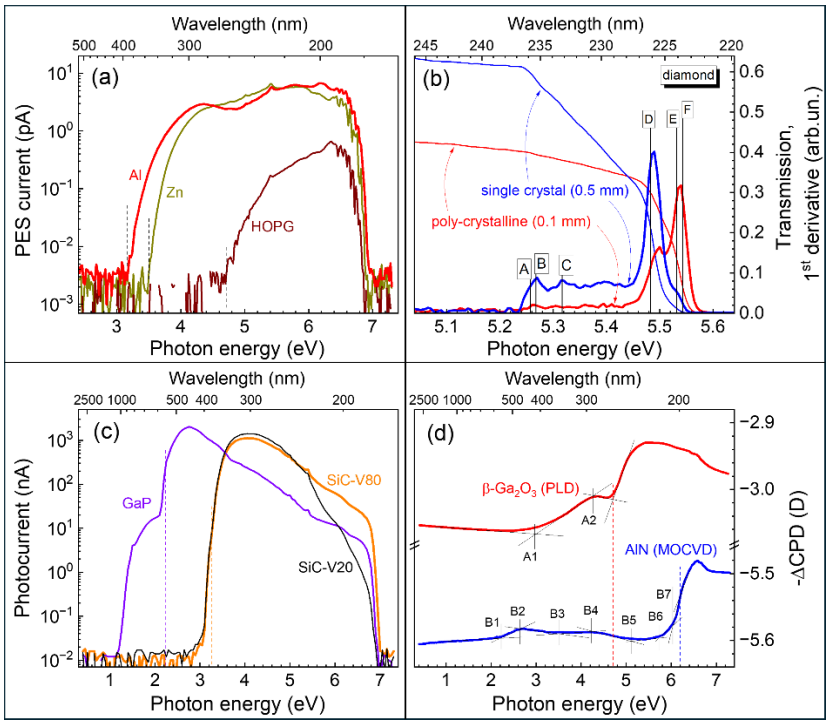

Fig. 4. Examples for applications of the mirrorless fused silica based double-prism monochromator: spectra of the photoelectron emission current of Al, Zn highly ordered pyrolytic graphite (HOPG) in air (red, green and brown lines, respectively, (a)). The dashed lines mark the corresponding work functions; spectra of the transmission (thin lines) and its first derivatives (thick lines) of a diamond single crystal (thickness 1mm, blue lines) and of polycrystalline

diamond (thickness 0.1 mm, red lines). The black lines at A, B, C, D, E and F mark the transitions near the indirect bandgap of diamond: E_g-E_x-$h\nu_{TO}$, E_g-E_x-$h\nu_{LO/LA}$, E_g-E_x-$h\nu_{TA}$, E_g-E_x+$h\nu_{TA}$, E_x+$h\nu_{LO/LA}$ and E_g-E_x+$h\nu_{TO}$ respectively (b); photocurrent spectra of photodiodes SiC-V20, SiC-V80 and GaP (black, orange and violet lines, respectively, (c)). The dashed orange and violet lines mark the bandgaps of SiC and GaP, respectively; and spectra of the contact potential difference of a β-Ga_2O_3 layer deposited by pulsed laser deposition (red line) and of an AlN layer deposited by MOCVD (blue line) (d).

Figure 4(a) shows photoelectron emission spectra (signals measured with a current amplifier, EMM) of freshly shaven with a steel knife Al and Zn and of delaminated HOPG (highly oriented pyrolytic graphite, SPI-1). The extracted values of the work functions of Al, Zn and HOPG in air were 3.16, 3.50 and 4.71 eV, respectively. For comparison, work functions of 3.1 – 3.2 eV [8] and 3.25 eV [9] were reported for Al after 1 min oxidation in air and a work function of 4.7 eV was found for delaminated HOPG [10]. Therefore, the application of the mirrorless fused silica based double-prism monochromator in combination, for example, with a LDLS gives the opportunity for measuring photoelectron emission spectra.

Figure 4(b) shows the transmission spectra and the spectra of their first derivatives of a 0.1 mm thin polycrystalline diamond window (type II, diamond materials) and of a 0.5 mm thick diamond (110) single crystal (elementsix) in the range around the indirect bandgap (5.47 eV). The samples were placed directly on the Si photodiode for the measurements. The slopes of the transmission spectra changed and several peaks were distinguished in the spectra of the derivatives whereas the thinner or thicker samples were more sensitive to the ranges of higher or lower photon energies, i.e. of stronger or weaker absorption, respectively. For comparison, the transition energies E_g-E_x-$h\nu_{TO}$, E_g-E_x-$h\nu_{LO/LA}$, E_g-E_x-$h\nu_{TA}$, E_g-E_x+$h\nu_{TA}$, E_g-E_x+$h\nu_{LO/LA}$ and E_g-E_x+$h\nu_{TO}$ are marked at 5.275, 5.268, 5.314, 5.482, 5.532 and 5.543 eV [11], respectively whereas E_g and E_x denote the indirect bandgap and the indirect exciton of diamond (E_g). The strongest changes of the absorption were present near the onsets of transitions. The transitions E_g-E_x-$h\nu_{TO}$ and E_g-E_x-$h\nu_{LO/LA}$, and the transitions E_g-E_x+$h\nu_{TO}$ and E_g-E_x+$h\nu_{LO/LA}$, were not separated in the measured spectra due to the limited spectral resolution. Therefore, the mirrorless fused silica based double-prism monochromator can be well used for optical spectroscopy in the DUV but one shall keep in mind the limited spectral resolution.

Photocurrent spectra are compared for one GaP and two SiC photodiodes in Figure 4(c) over the full range of photon energies. Photocurrents were measured with a low noise current amplifier (DLPCA-200, Femto). For the given GaP photodiode, photocurrents set already on at 1.15 eV, i.e. at photon energies far below the bandgap. Near the indirect bandgap of GaP (2.26 eV [12]), the photocurrent increased steeply by about 14 times at the bandgap and by more than 100 times in the maximum at 2.75 eV (bandgap of 4HC-SiC: 3.26 eV [13]). For the SiC-V20 and SiC-V80 photodiodes, the photocurrents set on about 2.7 and 2.8 eV, respectively, whereas the defect related photocurrents were larger for the SiC-V20 photodiode. Furthermore, the defect related photocurrents of the SiC photodiodes were lower by more than 2 orders of magnitude in comparison to the GaP photodiode. Around 4 eV, the photocurrent of the SiC-V80 photodiode was lower than the photocurrent of the SiC-V80 photodiode by about 20% but more than 4 times higher around 6 eV, i.e. bulk and surface recombination processes are rather different for both photodiodes. Therefore, optoelectronic devices can be characterized relatively fast and with a compact set-up over a huge spectral range.

Surface photovoltage spectra shown in figure 4(d) were measured in the Kelvin probe regime (see for details in the set-up [14]) on a β-Ga_2O_3 layer deposited onto sapphire by PLD (pulsed laser deposition) and on an AlN layer deposited onto sapphire by MOCVD (metal organic chemical vapor deposition). The change of the negative contact potential difference (-ΔCPD) under illumination corresponds to the surface photovoltage. The change of the signals towards more positive (negative) values of -ΔCPD means that photogenerated electrons (holes) and holes (electrons) are separated preferentially towards the back (front) and front (back) of the sample, respectively. Changes in the slope of -ΔCPD signals are related to the onset of a

transition whereas the direction of the change of the slope gives information about the direction of charge separation. Aside the pronounced onsets at the bandgaps of β-Ga_2O_3 (4.52 and 4.79 eV depending on polarization [15]) and AlN (6.2 eV [16]), defect related transitions, denoted by A1 and A2 for the β-Ga_2O_3 layer and B1 – B7 for the AlN layer, were observed at 2.95 and 4.27 eV for the β-Ga_2O_3 layer and at 2.22, 2.65, 3.50, 4.22, 5.12, 5.74 and 6.03 eV for the AlN layer, respectively. These defect related transitions can be compared, for example, with defect states in β-Ga_2O_3 or AlN obtained by other techniques (see, for example, [17] or [18], respectively). Therefore, the application of the mirrorless fused silica based double-prism monochromator allows for the study of defect transitions even in semiconductors with ultra-wide bandgap continuously over a very broad spectral range.
As a remark, regarding the time needed for the measurement of spectra, it shall be mentioned, that it took about 7, 1, 5 and 4 s for one measurement point in the spectra shown in figure (a), (b), (c) and (d), respectively. Depending on the number of measurement points, a spectrum is usually measured within 10 – 30 min with the mirrorless fused silica based double-prism monochromator.

6. Conclusions

A mirrorless fused silica based double-prism monochromator has been developed for a spectral range between 0.4 and 7.3 eV at the compromise between high light intensity, very low straylight, continuous measurement and intermediate spectral resolution. With regard to this, the mirrorless fused silica based double-prism monochromator is especially predestinated as a light source for photoelectric measurements. The mirrorless fused silica based double-prism monochromator is a new type of monochromator with a broad application potential. It can be applied, for example, for photoelectron, optical, photocurrent and surface photovoltage spectroscopy by using the same monochromator. For the first time, the developed mirrorless fused silica based double-prism monochromator opened the opportunity for robust photoelectric characterization over most of the range of bandgaps of semiconductors with ultra-wide bandgap what is of interest for applications in research and development as well as in industry.

Funding. This Project was supported by the Federal Ministry for Economic Affairs and Climate Action (BMWK) on the basis of a decision by the German Bundestag (for the authors T.D. and S.F. and for Freiberg Instruments: ZIM-project numbers KK5085302DF0, KK5123601DF0, KK5138401DF0, respectively).

Acknowledgements. The authors are grateful to L. Korte for discussions and support with a photodiode calibrated in UV/DUV by the PTB, to N. Papathanasiu (sglux GmbH) for discussions and for providing the SiC and GaP photodiodes, to N. Nickel for discussions and providing the β-Ga_2O_3 layer and to E. Richter (Ferdinand Braun Institute) and T. Wernicke (TU Berlin) for discussions and for providing the epitaxial AlN layer. Further the authors are grateful to N. Schüler (Freiberg Instruments) for critical reading of the manuscript.

Disclosures. The authors declare no conflicts of interest.

Data availability. Data underlying the results presented in this paper are not publicly available at this time but may be obtained from the authors upon reasonable request.

References

1. see, for example, F. Kohlrausch, Praktische Physik, B. G. Teubner, Stuttgart, 22nd Edition, 1968,
2. F. Nürnberg, B. Kühn, A. Langner, *et al*., „Bulk damage and absorption in fused silica due to high-power laser applications“, Proc. SPIE **9632**, 96321R 1–10 (2015).
3. I. H. Malitson, „Interspecimen comparison of the refractive index of fused silica“, J. Opt. Soc. Am. **55**, 1205–1209 (1965).
4. O. Schiek and E. Winter, “Two new mirror monochromators”, Appl. Optics **4**(2), 195-199 (1965).
5. T. Dittrich and S. Fengler, “Monochromator sowie Verfahren zur Monochromatisierung elektromagnetischer Strahlung”, EP 4 269 963 A1 (28.42022).

6. T. Dittrich, M. Franke, and S. Fengler, “Elektrische Schaltung zur Ermittlung einer elektrischen Stromstärke eines elektrischen Stroms und Verfahren zur Ermittlung einer elektrischen Stromstärke eines elektrischen Stroms unter Verwendung der elektrischen Schaltung“, DE102023003991.8 (22.9.2023).
7. R. E. Huffman, “Absorption cross sections of atmospheric gases for use in aeronomy”, Canadian J. Chem. **47**, 1823–1834 (1969).
8. Yu. I. Semov, “Work function of oxidized metal surfaces and estimation of Al_2O_3 film band structure parameters”, phys. stat. sol. **32**, K41–K44 (1969).
9. M. Uda, Y. Nakagawa, T. Yamamoto, *et al*., “Successive change in work function of Al exposed to air”, J. Electr. Spectr. Rel. Phen. **88**-**91**, 767–771 (1998).
10. W. N. Hansen, G. J. Hansen, „Standard reference surfaces for work function measurements in air“, Surf. Sci. **481**, 172–184 (2001).
11. C. D. Clark, P. J. Dean, and P. V. Harris, “Intrinsic edge absorption in diamond”, Proc. R. Soc. Lond. A **277**, 312–329 (1964).
12. M. B. Panish and H. C. Casey, “Temperature dependence of the energy gap in GaAs and GaP”, J. Appl. Phys. **40**, 163-167 (1969).
13. P. Ščajev and K. Jarašiūnas, “Application of a time-resolved four-wave mixing technique for the determination of thermal properties of 4H-SiC crystals”, J. Phys. D: Appl. Phys. **42**, 055413 1–6 (2009).
14. T. Dittrich, S. Fengler, and N. Nickel, „Surface photovoltage spectroscopy over wide time domains for semiconductors with ultrawide bandgap: example of gallium oxide“, Phys. Stat. Sol. **218**, 2100167 1–11, (2021).
15. N. Ueda, H. Hosono, R. Waseda, *et al*., “Anisotropy of electrical and optical properties in β-Ga_2O_3 single crystals”, Appl. Phys. Lett. **71**, 933–935 (1997).
16. H. Yamashita, K. Fukui, S. Misawa, *et al*., “Optical properties of AlN epitaxial thin films in the vacuum ultraviolet region”, J. Appl. Phys. **50**, 896–898 (1979).
17. X. Zhu, Y.-W. Zhang, S.-N. Zhang, *et al*., „Defect energy levels in monoclinic β-Ga_2O_3“, J. Lumin. **246**, 118801 1–6 (2022).
18. C. M. Matthews, H. Ahmad, K. Hussain, *et al*., “Cathodoluminescence investigation of defect states in n- and p-type AlN”, Appl. Phys. Lett. **124**, 052102 1–5. (2024).

Appendix

Figure A shows an example of a screenshot of the ray-tracer program with simulated pathways of photons incoming at wavelength of 477 nm (corresponding photon energy 2.6 eV), block of parameters and resolution spectrum for the given parameters (widths of the external and internal slits 0.2 and 0.5 mm, respectively). Absorption by the ambient gas was not considered. The transmission coefficients were calculated as the ratio between the numbers of incoming photons obtained just behind the entrance slit of the monochromator and the outgoing photons obtained behind the exit slit of the monochromator. The insert of figure A shows transmission spectrum of the mirrorless fused silica based double-prism monochromator which has been simulated between 0.4 eV (3100 nm) and 7.3 eV (169.7 nm). The total number of photons was kept at 2000 for the given simulation. The transmission was about 1.6 % at 0.4 eV (3100 nm) and increased to 6.4 % at 0.7 eV (1771.4 nm). The transmission was above 19 % in between 6.0 eV (206.7 nm) and 7.0 eV (177.1 nm).

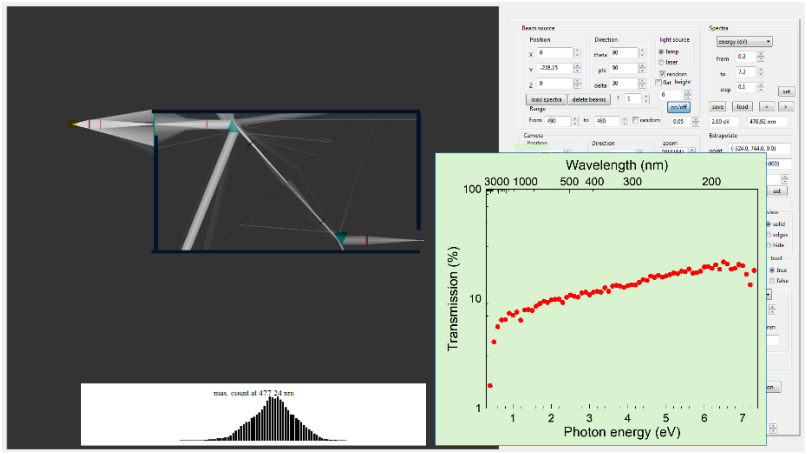

Fig. A. Example of a screenshot of the ray-tracer program with simulated pathways of photons incoming in the wavelength range between 460 and 490 nm while the monochromator was set to 477 nm (2.6 eV), block of parameters and resolution spectrum for the given parameters. The insert (red circles) shows the transmission spectrum of the monochromator (widths of the external and internal slits 0.2 and 0.5 mm, respectively).